American Journal of Physics and Applications
2021; 9(5): 102-109
http://www.sciencepublishinggroup.com/j/ajpa
doi: 10.11648/j.ajpa.20210905.11
ISSN: 2330-4286 (Print); ISSN: 2330-4308 (Online)

Femtosecond X-ray Lasers at λ=32.8 and 44.4 nm in a Plasma Formed by Optical Field Ionization in a Krypton Cluster Jet

Elena Ivanova

Institute of Spectroscopy, Russian Academy of Sciences, Moscow, Russia

Email address:
eivanova@isan.troitsk.ru

To cite this article:
Elena Ivanova. Femtosecond X-ray Lasers at λ=32.8 and 44.4 nm in a Plasma Formed by Optical Field Ionization in a Krypton Cluster Jet. *American Journal of Physics and Applications*. Vol. 9, No. 5, 2021, pp. 102-109. doi: 10.11648/j.ajpa.20210905.11

Received: July 15, 2021; **Accepted**: August 4, 2021; **Published**: September 10, 2021

Abstract: Due to high efficiency, X-ray lasers based on transitions of Ni-like krypton (Kr^{8+}) are being actively studied. The main focus is on an X-ray laser based on the conventional $3d_{5/2}4d_{5/2}$ [J=0] – $3d_{3/2}4p_{1/2}$ [J=1] transition at λ=32.8 nm. Gaseous krypton targets or krypton cluster jets are used in various experiments. X-ray lasers at 32.8 nm in a plasma formed by optical field ionization in a krypton cluster jet are widely used for research of nanoobjects. In this article, the possibility of creating an efficient X-ray laser in Ni-like krypton based on a transition with optical self-pumping $3d_{3/2}4f_{5/2}$ [J=1] – $3d_{3/2}4d_{5/2}$ [J=1] at λ=44.4 nm is predicted for the first time. The plasma filament is excited upon interaction of a jet of krypton clusters with an intense pump laser pulse. Optimal conditions to achieve the duration t_{las} ≤300 fs of the X-ray laser radiation are determined. The optimal electron density is in a rather narrow interval in the range $n_e \sim 10^{21}$ - 2×10^{21} cm^{-3}. The optimal electron temperature is several keV. It is likely that this explains the fact that no X-ray laser has been observed on this transition in Kr^{8+} so far. The conversion factor per pulse is found to be ~5×10^{-5}. For an X-ray laser operating on the conventional transition $3d_{5/2}4d_{5/2}$ [J=0] – $3d_{3/2}4p_{1/2}$ [J=1] at λ=32.8 nm, $t_{las} \leq 300$ fs can also be achieved; however, the conversion factor for this transition is times ~5 smaller than that for the former transition.

Keywords: X-ray Lasers, Optical Self-pumping X-ray Laser, Radiative-Collisional Model, Cluster Jets, Optimal Density, Electron Temperature in Nanoplasmas

1. Introduction

X-ray free electron lasers (XFELs) with λ=1-10 nm and a pulse duration (t_{las}) of the order of a hundred of femtoseconds allow recording holographic images of intermediate states of nano-objects at times comparable to the times of atomic motions [1-4]. These works demonstrate the possibility of observing the dynamics of phase transitions in solids – the formation of cracks, the nucleation and separation of phases, and rapid fluctuations in liquids and biological cells. Intense X-ray lasers (XRLs) with sub picosecond t_{las} can be used to diagnose very rapidly changing laser plasmas in the region of critical surface density.

In 2017, a new generation femtosecond XFEL came into commission in Hamburg [5]. The minimum t_{las} reached 100 fs, the pulse repetition rate of the XFEL was 27000 s^{-1}, and the wavelength varied in the range 0.05 – 6 nm. At present, intensive investigations are underway to determine the mechanisms of formation of toxic proteins responsible for the formation of diseases of various kinds.

Experiments [6-9] have demonstrated the fundamental advantage of using cluster jets as targets for creating high-temperature plasmas. The plasma is pumped by intense pulses of femtosecond lasers; the plasma formation mechanism is the optical field ionization (OFI). Let us list the main prerequisites for using the OFI method for cluster targets to create highly efficient X-ray lasers in cluster jets: (i) The target can absorb of up to ~ 90% of the pump energy due to weak reflection; in this case, the plasma does not contain any fragments and oxides. (ii) Electrons are capable of achieving energies on the order of tens and hundreds of thousands of keV. (iii) The plasma density is controlled by the size and number of clusters. (iv) The ionization balance is controlled by the pump intensity I_{pump}; if the intensity I_{pump} is correct,

immediately after the interaction of the pump pulse with the target, a plasma is formed in which ~90% of all ions are formed in the state of the working ion of an X-ray laser (XRL). (v) A high degree of coherence of the output radiation of an XRL is possible if one uses a high-order harmonic with a wavelength close in value to λ of the XRL; a high-order harmonic is formed in the delay line and propagates simultaneously with the XRL pulse.

Ivanova [10, 11] developed a theoretical model of a sub picosecond XRL formed in a jet of xenon clusters upon interaction with an intense pump laser, where the gain of spontaneous emission on the 4d5d [J=0] – 4d5p [J=1] transition at λ=41.8 nm in Pd-like xenon (Xe^{8+}) was determined. It is important to note that the results of calculations of Ivanova [11] for low temperatures were confirmed by subsequent experimental results performed by Mocek et al [12].

In the work of Ivanova and Vinokhodov [13], a model of an X-ray laser based on the conventional $3d_{5/2}4d_{5/2}$ [J=0] – $3d_{3/2}4p_{1/2}$ [J=1] transition with λ=32.8 nm in Ni-like krypton (Kr^{8+}) was calculated. In this work, the known experimental measurements of quantum yield of an XRL on this transition were interpreted. In various experiments, the plasma was pumped in gaseous krypton and in a jet of krypton clusters. For the jet of clusters, optimal conditions were found under which the saturation of the quantum efficiency along the plasma length was ~ 300 μm (that corresponds to the XRL pulse duration t_{las}~ 1 ps). Under optimal conditions, the density of krypton atoms was $n_{Kr} \sim (4\text{-}9)\times10^{19}$ cm^{-3} and the electron temperature was $T_e \sim 5000$ eV. The conversion factor was ~ 5×10^{-3} of the pump pulse energy. Ivanova and Vinokhodov [13] proposed a detailed schematic diagram of the experimental setup of a highly efficient XRL formed in a jet of krypton clusters. A similar scheme was implemented in the experiment of Sebban et al [14], where a Ni-like krypton plasma was created by the method of OFI of krypton atoms. In this experiment, a circularly polarized pump laser beam was focused either into a cell with gaseous krypton or into a jet of gaseous krypton; the XRL on the conventional $3d_{5/2}4d_{5/2}$ [J=0] – $3d_{3/2}4p_{1/2}$ [J=1] transition with λ=32.8 nm in (Kr^{8+}) was studied. In the experiment of Sebban et al [14] it was shown that the dynamics of the output XRL pulse can be controlled by using a pulse of a high-order harmonic that is focused into the gain medium; the high-order harmonic wavelength is close to the XRL wavelength. By stretching the time of the high-order harmonic pulse to the gain duration g(t), continuous and coherent XRL emission can be achieved. It was found [14] that, as the plasma electron density increased from $n_e=3\times10^{18}$ to $n_e=1.2\times10^{20}$ cm^{-3}, the XRL radiation duration t_{las} decreased from 7 ps to 450 fs. The duration t_{las} was defined as the full width at half maximum (FWHM) of the XRL radiation pulse intensity.

2. Formulation of the Problem

Figure 1 shows the scheme of an XRL that operates on two conventional transitions 3d4d [J=0] - 3d4p [J=1] in the Kr^{8+} ion. The ground state of a Ni-like ion is a closed shell of the $3d^{10}$ [J=0] core. The classification of levels is presented in the j-j coupling scheme of the angular momenta. An excited state of the ion is presented by the state of a vacancy in the core ($3l_j$) and by the state of an electron above the core ($4l_j$). The transition $3d_{5/2}4d_{5/2}$ [J=1] - $3d_{3/2}4p_{1/2}$ [J=1] with λ=32.8 nm is strong. The XRL transition whose inversion is caused by the optical self-pumping (OSP) $3d_{3/2}4f_{5/2}$ [J=1] – $3d_{3/2}4d_{5/2}$ [J=1] at λ=44.4 nm is also presented.

Physical principles of an XRL with OSP have been presented by Nilsen et al [15, 16]. In fact, an XRL with OSP is an alternative approach to the conventional radiative collisional model. In the conventional model, the upper working level is populated from the ground level at a high rate due to its monopole excitation by electron impact, it radiatively decays only into lower working levels (radiative decay into the ground state is forbidden); the population inversion of the working levels occurs due to the rapid decay of the lower working level into the ground state (see Figure 1).

The inversion of XRL working levels under the OSP conditions is due to a high rate of population of the upper working level by means of dipole excitation by electron impact, as well as reabsorption of radiation from the upper working level $3d_{3/2}4f_{5/2}$ [J=1] to the ground state $3d^{10}$ [J=0]. The reabsorption of radiation manifests itself in the fact that the effective radiative decay of the upper level into the ground state in an optically dense plasma is much smaller than in an isolated ion. In our model, the plasma appears to be stable and quasi-stationary, and mass transfer is not taken into account. In this case, the reabsorption of radiation can be taken into account by the Biberman-Holstein factor - the escape factor G, which determines the ratio of the effective rate of radiative decay of an ion in plasma ($A^{eff}_{j\text{-}0}$) to the rate of radiative decay of an isolated ion ($A_{j\text{-}0}$): $A^{eff}_{j\text{-}0}=G\cdot A_{j\text{-}0}$ (G <1). For an optically dense plasma, Fill [17] proposed the following form to calculate the escape factor G:

$$G=1.22[\ln(k_0 d)]^{1/2}/(k_0 d) \quad (1)$$

where κ_0 is the photon absorption coefficient, and d is the diameter of the cylindrical plasma.

A new class of XRLs based on OSP principles has been investigated experimentally by Nilsen et al [16] in Ni–like Zr^{12+}, Nb^{13+}, and Mo^{14+} ions. In this experiment, solid targets were used. Plasma was pumped by means of two laser pulses: preliminary (1 J, 600 ps), which was used to create the plasma, then the main pulse (5 J, 1 ps), which heated the plasma. The interval between the pulses was 700 ps. The laser pumping beams were focused into a line into a target, whose length was varied from 0.4 to 1 cm. The emission XRL spectra are shown in Figure 2 from the reference [16], where one can see high-intensity XRL lines for the conventional and OSP transitions.

Progress in the study of XRLs based on the OSP mechanism was observed in a subsequent experiment performed by Kuba et al [18], where a sub picosecond heating pulse was used to pump plasma from a solid silver target. In this experiment, conditions for achieving a strong laser effect on an OSP transition in Ag^{19+} were determined. In a recent experimental

work of Siegrist et al [19], the OSP mechanism was investigated in Ni-like ions, such as Ru^{16+}, Pd^{18+}, and Ag^{19+}. In this experiment, XRL lines based on the OSP mechanism were experimentally observed in Ne-like ions, such as V^{13+}, Cr^{14+}, Fe^{16+}, and Co^{17+}.

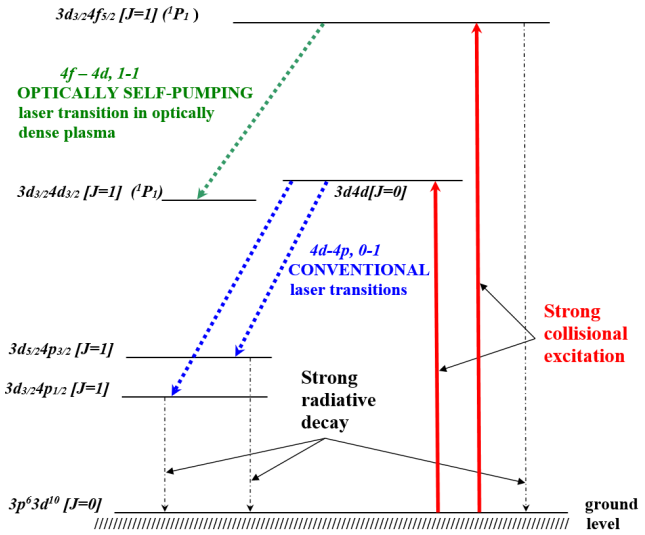

Figure 1. *The scheme of XRL transitions in Ni-like krypton (Kr^{8+}): the conventional transition $3d_{5/2}4d_{5/2}$ [J=0] – $3d_{3/2}4p_{1/2}$ [J=1] at λ=32.8 nm and the optical self-pumping transition $3d_{3/2}4f_{5/2}$ [J=1] – $3d_{3/2}4d_{5/2}$ [J=1] at λ=44.4 нм.*

Ivanova [20] presents results of calculations of the wavelengths of XRL transitions based on the OSP principles for Ni–like ions sequence with Z≤ 79. The calculations were performed using relativistic perturbation theory with a model potential of zero-approximation (RPTMP) by Ivanova [21].

Neither calculations of Ivanova [13] nor experiment of Sebban et al [14] have not considered the gain due to the OSP transition in Ni-like krypton at λ=44.4 nm. Below we will calculate a theoretical model of an XRL with λ=32.8 nm and λ=44.4 nm in a plasma formed upon interaction of a femtosecond pump laser with a jet of krypton clusters. The goal of the calculation is: (i) to determine plasma parameters, pumping conditions, and basic principles of an experiment to achieve the duration of the output XRL radiation ≤ 300 fs; (ii) for each transition, to calculate the dependences of energy yields of the XRL on the plasma density.

3. Evolution of the Gain of an XRL at λ=32.8 nm and λ=44.4 nm Under Optimal Conditions

Under the assumption that plasma is homogeneous and free of impurities, five parameters are sufficient to describe it: the temperatures and the densities of electrons and ions, T_e, T_i, n_e, and n_i, and the diameter of the plasma filament d. It was shown by Ivanova [10, 13] that the shape of the T_e distribution practically does not affect the calculation results. To calculate the gain g at the center of an XRL line, we will use the well-known expression proposed by Whitney et al [22]:

$$g=A_{ul}\lambda^2(N_{up} - (g_{up}/g_{low})N_{low})/8\pi\Delta\nu_0 \quad (2)$$

where A_{ul} is the probability of a radiative transition from the upper to the lower working level, λ is the transition wavelength, N_{up} and N_{low} are the numbers of atoms per unit volume in the upper and lower working states, respectively, g_{up} and g_{low} are the statistical weights of the upper and lower working levels, respectively. The shape of the transition line is determined by the convolution of the intrinsic and Doppler contours. The intrinsic contour is determined by radiative transitions and collisional processes, which connect each of the levels with all other levels of the working ion, as well as with the levels of the ion of the adjacent stage of ionization. The line width at the center (Voigt profile) $\Delta\nu_0$ is determined by a simplified method, which was developed by Whitney et al [22].

The calculations will assume the following.

1) The plasma is formed in the shape of a cylinder with diameter d and length L as a result of propagation of a laser pumping pulse through a beam of clusters with thickness L.
2) The parameters of the pump pulse are such that, immediately after the end of the interaction of the optical field of the laser with clusters, the plasma is formed with an electron temperature T_e, in which the Kr^{8+} ions constitute ~90% and reside in the ground state.
3) The temperatures of electrons (T_e) and ions (T_i), as well as the plasma diameter (d), are homogeneous throughout the volume and remain unchanged during the emission time of the XRL.
4) The energy distributions of electrons and ions are assumed to be Maxwellian, and the shape of the distribution does not play a significant role in calculations of the rates of transitions induced by electron-ion collisions.
5) The temperatures of ions and electrons in the plasma are the same, $T_i=T_e$.
6) We will not calculate the dynamics of gain of spontaneous radiation propagating in the plasma; here, one of possible approaches is to solve the Maxwell-Bloch equations developed by Kim et al (see e.g. [23]). Such calculations are necessary to determine the saturation of g(t) along the plasma length L. In the case considered here (as well as in the overwhelming majority of experiments), the gain is observed in the ionization regime of the working ion in the state of a higher stage of ionization. In principle, the lifetime of the working ion in the plasma determines the value of L.
7) In the calculation, we will average the gain g(t) over the spatial and temporal coordinates. For this purpose, we will divide the target-cylinder into segments that are shorter than the length of the spatial scale of the pump pulse; then, elementary processes in each segment will proceed identically, but with some time delay. In this case, it is sufficient to perform only the time averaging for the function g(t).

In addition to Figure 1, Table 1 presents spectroscopic characteristics (rate coefficients of kinetic equations) for two XRL transitions. The probabilities of radiative transitions (PRTs) in the table are given for an isolated ion. Figure 2

graphically shows the PRTs of two working levels: $A^{eff}_{low\text{-}0}$ for the lower working level of the conventional transition and $A^{eff}_{up\text{-}0}$ for the upper working level of the OSP transition to the ground state of the Kr^{8+} ion in relation to the electron density. The calculation was carried out taking into account formula (1) at d=25 μm and T_e=10000 eV. Figures 3a and 3b show the temperature dependences of the electron impact excitation rates of the upper and lower working levels of both transitions. The calculation was performed by the RPTMP method according to the formulas derived by Ivanov et al [24].

Below, we will explain why a significant inversion of the rapidly decaying upper level $3d_{3/2}4f_{5/2}$ [J=1] of the OSP transition is possible with respect to the $3d_{3/2}4d_{5/2}$ [J=1] lower level, which is practically stable against radiative decay (see Table 1).

Figure 2 demonstrates that the rates of radiative decay of the lower working level of the conventional transition ($A^{eff}_{low\text{-}0}$) and the upper working level of the OSP transition ($A^{eff}_{up\text{-}0}$) to the ground state of the Kr^{8+} ion significantly decrease with increasing density. At the optimal density $n_e=1.5\times10^{21}$ cm^{-3} (which will be defined below), $A^{eff}_{up\text{-}0} \sim 10^{10}$ s^{-1}; in this case, the population of the upper OSP level is P_{up}=0.07. Radiation depletion of this level in kinetic equations is given by $P_{up}\times A^{eff}_{up\text{-}0}=7\times10^8$ s^{-1}.

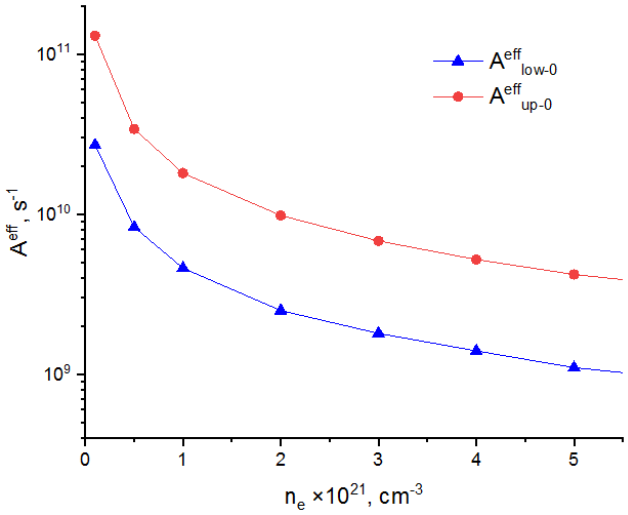

Figure 2. *Probability of the radiative transitions from the lower working level $A^{eff}_{low\text{-}0}$ of the conventional XRL transition and from the upper working level $A^{eff}_{up\text{-}0}$ of the OSP transition to the ground state of Kr^{8+}. Dependence on n_e is given at d=25 μm, T_e=10000 eV.*

Table 1. *Spectroscopic characteristics for two XRL transitions.*

	Conventional transition		**Optically self-pumping transition**	
	Upper level	**Lower level**	**Upper level**	**Lower level**
	$3d_{5/2}4d_{5/2}$ [J=0]	**$3d_{3/2}4p_{1/2}$ [J=1]**	**$3d_{3/2}4f_{5/2}$ [J=1]**	**$3d_{3/2}4d_{5/2}$ [J=1]**
E (eV)	144.85	107.13	164.32	136.42
λ (nm)	32.8		44.4	
E_{tr} (eV)	37.7		27.9	
$A_{low\text{-}0}$ (s^{-1})		7.25E+10		2.0 E+05
$A_{up\text{-}0}$ (s^{-1})	0.00+00		6.4 E+11	
$A_{up\text{-}low}$ (s^{-1})	1.8 E+10		5.6 E+09	
R_{col}^{up} (cm^{-3} s^{-1})	7.0 E-10		0.8 E-10	
R_{col}^{low} (cm^{-3} s^{-1})		3.0E-10		2.0 E-13
$\Delta\nu_0$ (s^{-1})	1.4 E+13		9.0 E+12	

Designations: E (eV) - energy level above the closed shell $3d^{10}$; λ (nm) - wavelength of the XRL transition; E_{tr} (eV) – XRL transition energy; $A_{low\text{-}0}$ (s^{-1}) –PRT of the low working level to the ground state; $A_{up\text{-}0}$ (s^{-1}) - PRT of the upper working level to the ground state; $A_{up\text{-}low}$ (s^{-1}) – PRT of the upper working level to the low working level. PRT are given for the isolated level Kr^{8+}.
R^{up}_{Col} (cm^{-3} s^{-1}), R^{low}_{Col} (cm^{-3} s^{-1}) – electron impact excitation rates per unit volume of the upper and lower working levels, respectively; $\Delta\nu_0$ (s^{-1}) – Voight width at the center of the transition line – are calculated at T_e=10000 eV, d=25 μм; for each transition, the value $\Delta\nu_0$ is calculated at optimal n_e.

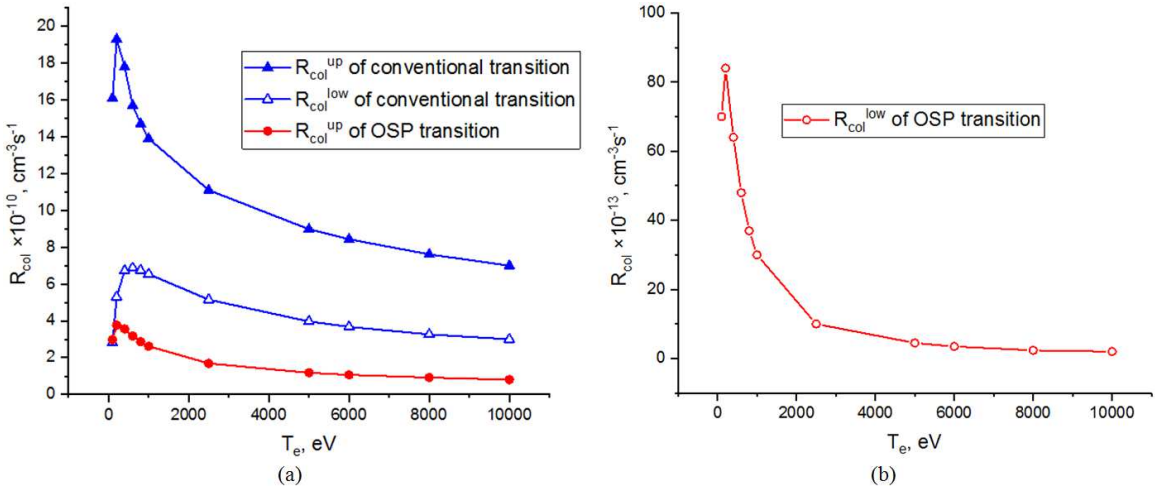

Figure 3. *Electron impact excitation rates per unit volume of the upper R_{col}^{up} and low R_{col}^{low} working levels of the conventional transition and upper R_{col}^{up} OSP transition (a); low working level R_{col}^{low} OSP (b) depending on T_e.*

The rates of the electron impact excitation of levels from the ground state of the Kr^{8+} ion, R_{col}^{up} and R_{col}^{low}, increase in proportion to the density. At optimal $n_e=1.5\times10^{21}$ cm^{-3} for the OSP transition, the population of the upper level by electron impact in the balance equations: $R_{col}^{up} \times n_e \times P_0=10^{-10} \times 1.5\times 10^{21} \times 0.55=8.3\times10^{10}$ s^{-1}, where $P_0=0.55$ is the population of the ground level at the optimal n_e. Therefore, due to the optical self-pumping (reabsorption) and a high rate of collisional population, the population of the upper level of the OSP transition is ~2 orders of magnitude higher than the radiative decay. Figure 3b shows that the population of the lower level of the OSP transition is 2.5 orders of magnitude smaller than the population of the upper level, which provides a large value of inversion of this transition at optimal n_e. Because the lower working level is populated weakly, the inversion of the SPP transition takes place in the entire range of the considered densities.

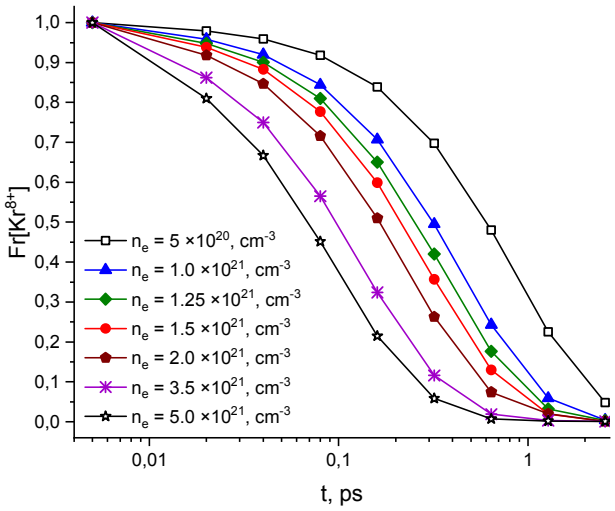

Figure 4. *Reduction of the fraction of the working ion Fr [Kr^{8+}] in the plasma due to ionization in higher ionization stages.*

The kinetic equations take into account the states of two ions of adjacent ionization stages; all radiative-collisional processes coupling two adjacent ions are taken into account in the kinetic equations. These processes and methods for their calculation were presented by Ivanov et al [25]. In this approach, it is possible to calculate the evolution of the gain coefficient taking into account the ionization of the working ion. The ionization time actually determines the duration of the XRL pulse. Figure 4 shows the time dependence of the fraction of working ions Fr [Kr^{8+}] in the plasma for different n_e.

For sub-picosecond XRLs to be efficient, it is necessary that the average value of the gain coefficient was $\bar{g}(t) \sim 1000$ cm^{-1}. Preliminary calculations of Ivanova and Zinoviev [26] show that the value of g(t) with λ=32.8 nm and λ=44.4 nm in Ni-like krypton increases extremely rapidly with increasing electron temperature T_e. Rapid growth takes place at relatively low T_e; see Figure 3a for the rates of excitation by electron impact.

A large number of parameters that characterize (a) plasma and its geometry; (b) nozzle, pressure in the gas reservoir, and size of clusters; and (c) laser pump pulse should be consistent with the theoretical model. Then the active medium, in principle, can be created using only one main pump pulse. This is possible if the model adequately reproduces the results of experiment. Ivanova and Vinokhodov [13] interpreted the experimental results on the observation of gain and quantum yield of XRL with λ=32.8 nm in gaseous krypton and in a jet of clusters; the comparison with them demonstrated the correctness of our model.

First experiments on the creation of high-temperature plasmas upon interaction of an intense pump laser pulse with a jet of xenon clusters demonstrated the achievement of electron temperatures on the order of a few keV [27-28]. Ditmire et al demonstrated [29], that maximum ion temperatures in their experiment were $T_i^{max} \geq 1$ MeV. In later works of Ditmire et al [30], it was shown that the size of the cluster is important for the formation of a high-temperature plasma upon interaction of an ultrashort pump pulse with a jet of clusters. The pedestal of the pulse is usually several nanoseconds; during the interaction of the pulse pedestal with the cluster, the cluster is heated, electrons escape from its surface, and the cluster expands. The largest values of T_e and T_i are achieved when the electron density n_e in the cluster nanoplasma is $3\times n_{crit}$ ($n_{crit}=\pi c^2 m_e/e^2\lambda^2$): the laser frequency is equal to the plasma frequency; in this case, the laser energy is resonantly contributed to the plasma energy. To achieve the maximum energy contribution, the duration and intensity of the pedestal should correspond to the cluster size: if a cluster is too small (expands rapidly, reaching $3\times n_{crit}$), it collapses too quickly (prior to the arrival of the main intense pulse), and the plasma T_e is not high. If a cluster is too large (it expands for too long), it collapses after the passage of the intense pulse, and T_e of the plasma is also not high. A cluster of the correct size reaches $n_e=3\times n_{crit}$ at the moment of time of the arrival of the main femtosecond pump pulse; in this case, a maximum contribution of a pump pulse energy to the nanoplasma temperature becomes possible.

The sizes of clusters as functions of the pressure and temperature of the gas in the initial chamber, as well as of the geometry of the valve, have been well studied for cone-shaped valves with round holes, for which the number of atoms in noble gas clusters is usually determined by the Rayleigh scattering method using the empirical formula given by Hagena and Obert [31]. Chen et al [32] studied the dependences of the cluster sizes on gas pressure in the initial chamber for a slotted nozzle. In this experiment it was shown that a slotted supersonic nozzle provides a significantly higher number of atoms in a cluster as compared to a cone-shaped nozzle.

The dependences of the energies of electrons and ions in plasma on cluster size were studied in many experiments, e.g., by Shao et al [28] and by Springate et al [33]. In the experiment [28], a jet of xenon clusters was irradiated by a

laser with a peak intensity of 2×10^{16} W/cm^2 and with a pulse energy of 30 mJ; it was shown that the clustering of xenon atoms with increasing pressure in the initial chamber begins at a pressure of ~ 1 bar. With increasing pressure, the size of the cluster increases, which leads to a rapid increase in the electron temperature in the plasma (see Figure 2 in the reference [28]). The plot of the growth of T_e with increasing density qualitatively coincides with the result obtained by Ivanova [10], which was shown in Figure 4 of that work. To continue this plot into the range of high plasma densities ($n_i \geq 10^{18}$ cm^{-3}, which corresponds to a cluster size of $\geq 10^3$ atoms/cluster), we will use Figure 4 from the reference [10], as well as plots from the experiment [33]. The resulting plot of T_e versus n_i was shown in Figure 6 of the calculation [13]. The inset of Figure 6 of the calculation [13] shows the corresponding dependence of T_e on the cluster size for Xe and Kr. We used this dependence to calculate the gain g(t) in the work [13]. As can be seen from the plots of Figure 6 from the calculation [13], for Kr clusters, T_e drops at larger cluster sizes (larger values of n_{Kr}). As will be shown below in this work, to create XRLs of sub-picosecond duration, it is assumed that the pump pulse intensity is 5×10^{17} W/cm^2, while the pulse energy is 0.16 J. The corresponding T_e values are at least one and a half orders of magnitude higher than those in the experiment [28].

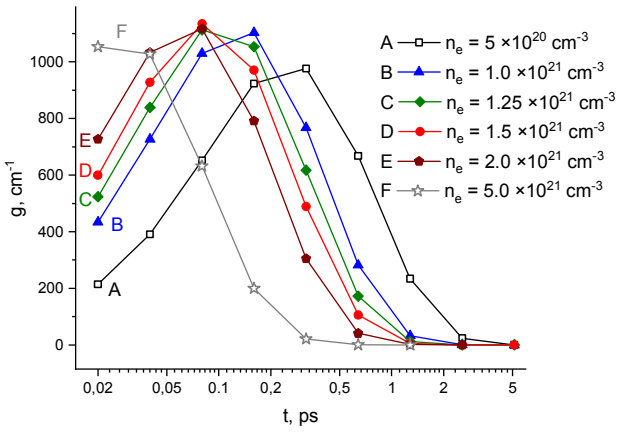

Figure 5. *Gain evolution of the XRL at λ=32.8 nm in plasma with T_e=10 keV, d=25 μm and electron density in the range $5\times10^{20} \leq n_e \leq 5\times10^{21}$ cm^{-3}.*

Based on the convenience of focusing the pump pulse, we will assume that the diameter of the plasma filament is d=25 μm. The length L=100 μm was selected from the condition that the XRL pulse duration is $t_{las} \leq 300$ fs. Figures 5 and 6 show the evolution of the gain for the conventional transition at λ=32.8 nm and the transition with OSP at λ=44.4 nm, respectively. The plots demonstrate dependences g(t) at different plasma densities. The electron density of the plasma varies within $5\times10^{20} \leq n_e \leq 5\times10^{21}$ cm^{-3}. In order not to clutter Figures 4-10, weak transitions are indicated by blank operators. Figures 7 and 8 show the dependences of the quantum yields of XRLs at the same plasma densities. The plot of Figure 7 shows that, for the conventional transition with λ=32.8 nm, the optimal density is $n_e=1.25\times 10^{21}$ cm^{-3}, and the density of krypton atoms ~ n_{Kr} ~1.5×10^{20} cm^{-3}. The plot of Figure 8 shows that, for the transition with λ=44.4 nm, the optimal density is $n_e=1.5\times10^{21}$ cm^{-3}, while the density of krypton atoms $n_{Kr} \sim 1.9\times 10^{20}$ cm^{-3}.

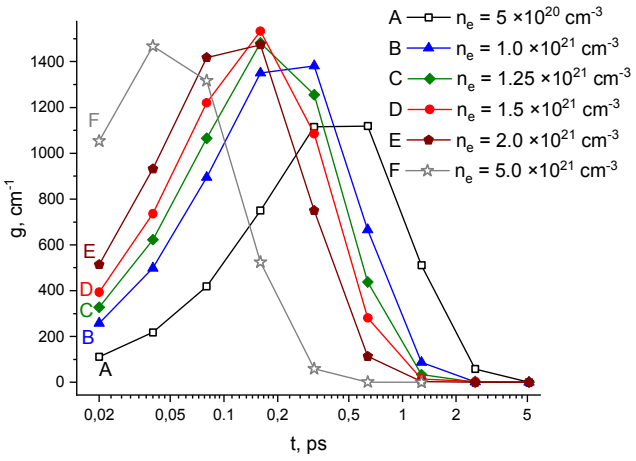

Figure 6. *Gain evolution of the XRL at λ=44.4 nm in plasma with T_e=10 keV, d=25 μm and electron density in the range $5\times10^{20} \leq n_e \leq 5\times10^{21}$ cm^{-3}.*

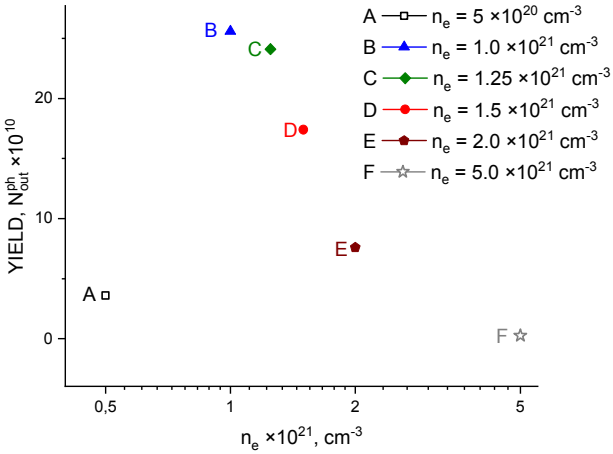

Figure 7. *Quantum yield of XRL at λ=32.8 nm in plasma with T_e=10 keV, d=25 μm, and electron density in the range $5\times10^{20} \leq n_e \leq 5\times10^{21}$ cm^{-3}.*

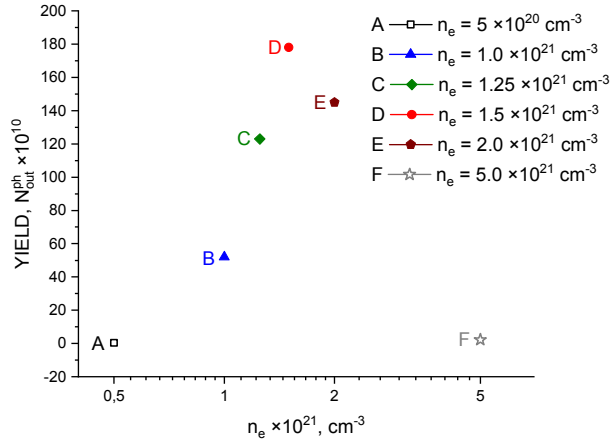

Figure 8. *Quantum yield of XRL at λ=44.4 nm in plasma with T_e=10 keV, d=25 μm, and electron density in the range $5\times10^{20} \leq n_e \leq 5\times10^{21}$ cm^{-3}.*

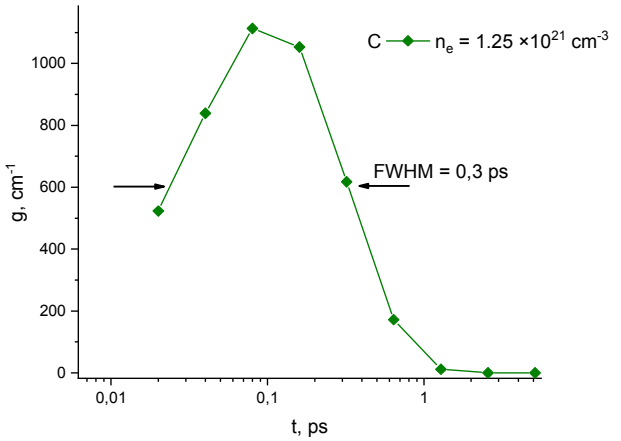

Figure 9. *The XRL pulse width at half maximum for the transition at λ=32.8 nm in plasma with T_e=10 keV, d=25 μm, and electron density n_e=1.25×10^{21} см$^{-3}$. C is designation of the line in Figures 5-8.*

The occurrence of maxima in the functions N_{out}^{ph} (n_e) at constant T_e and d (see Figures 7, 8) can be easily understood. At small n_e, an increase in the density leads to an increase in g(t), since the number of working ions, ions with the population inversion of working levels, increases. With a further increase in n_e, the collisional mixing of the level populations is enhanced, which leads to a decrease in the inversion. Therefore, for the XRL with λ=44.4 nm, optimal values of n_e lie in a rather narrow interval in the range $n_e \sim 10^{21} - 2\times10^{21}$ cm^{-3}. It is likely that this explains the fact that no XRL has been observed on this transition so far. Let us calculate the intensity I_{pump} and duration t_{pump} of a pump laser of a cluster target with the volume $V=5\times10^{-8}$ cm^3 and electron density in the plasma $n_e=1.5\times10^{21}$ cm^{-3}. The amount of the absorbed energy in the volume V is $E_{pump}\sim10^{18}$ eV. Then, t_{pump}=40 – 50 fs, $I_{pump}=5\times10^{17}$ W/cm^2. The energy output of an XRL pulse with λ=44.4 nm is $E_{out}=1.8\times10^{12}\times27.4=5\times10^{13}$ eV (see Figure 8). The energy output of an XRL pulse with λ=32.8 nm is $E_{out}=2.5\times10^{11}\times37.7=9.4\times10^{12}$ eV (see Figure 7); i.e., it is 5 times smaller than that on the OSP transition.

The XRL pulse width at half maximum for the transition with λ=32.8 nm is shown in Figure 9: FWHM=0.3 ps; for the transition with λ=44.4 nm, it is shown in Figure 10: FWHM=0.37 ps.

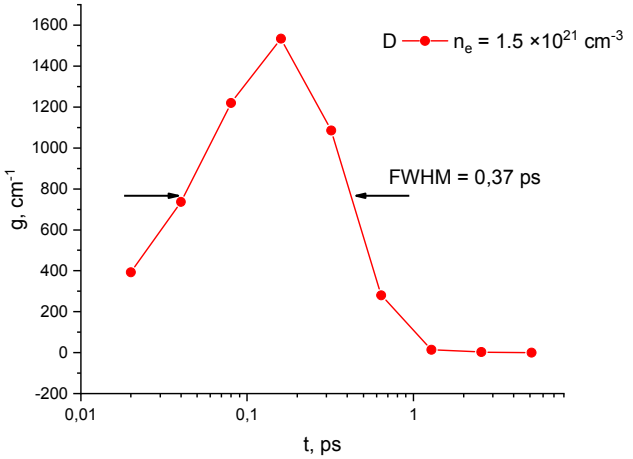

Figure 10. *The XRL pulse width at half maximum for the transition at λ=44.4 nm in plasma with T_e=10 keV, d=25 μm, and electron density n_e=1.5×10^{21} см$^{-3}$. D is designation of the line in Figures 5-8.*

4. Conclusion

A comparison of the technical characteristics of an XRL in krypton cluster jet and a new generation free electron laser is presented in Table 2.

Table 2. *Comparison of the characteristics of the XRL in krypton cluster jet with the FXEL of new generation in Hamburg.*

Characteristics	XRL in Krypton cluster jet	FXEL in Hamburg
Size	Small buildings	Length 3.5 km
Wavelength λ_{las}	44.4 and 32.8 nm	0.05 – 6 nm
Laser Pulse Repetition Rate	>10^5 /sec	2.7×10^4 /sec
The cost	From 1 million euro	1.5 billion euro
Service cost	Maintenance cost is relatively small	35000 euro per hour
Prevalence	Many installations possible	Unique installation in Europe
Shortest pulse duration (t_{las})	≤ 300 fs	~ 100 fs
Coherence	High degree of coherence is possible with using harmonics	Coherence allows resolution up to several tens of nanometres

In the model of a femtosecond XRL that was calculated here, it was proposed to use as a target a jet of krypton clusters emitted from a flat valve. The cluster size is ~ 50 nm. The pump laser intensity incident on the target is $I_{pump} \sim5\times10^{17}$ W/cm^2, $E_{pump}\sim10^{18}$ eV, and t_{pump}=40 – 50 fs. The pedestal of the pump laser should be selected preliminarily in order to achieve a maximum energy deposition.

The model of a femtosecond XRL with λ=32.8 nm and λ=44.4 nm that was calculated here has conversion factors of ~10^{-5} and 5×10^{-5}, respectively. For an XRL with λ=44.4 nm, the number of emitted photons was found to be ~ 2 × 10^{12} photons/pulse. This intensity of the XRL output radiation is, in principle, sufficient to achieve high quality single-pulse images of objects with sizes ≤100 nm [9]. At present, methods have been developed on the basis of works [6-9] for obtaining high-quality images of various nano-objects, although the XRL pulse duration there was tens of picosecond.

The duration of an XRL pulse can be made significantly shorter if optical shutters of the time-gating method proposed by Ivanova Vinokhodov [13] will be used; however, in this case, the efficiency will decrease. One of the advantages of an XRL in cluster jets is its high repetition rate of XRL pulse. In one of the first studies of plasma radiation produced upon interaction of an intense pump laser pulse with a jet of clusters

performed by Ter-Avetisyan et al [34], a pulse repetition rate of 1.2×10^5 Hz was experimentally demonstrated. Due to the fast-pumping rate of the cluster jet, the repetition rate can be significantly increased. In this case, it is possible to achieve a rate of $\geq 10^6$, at which the energy yield will be ~ 10 W.

In 2017, the first laser with a petawatt power (10^{15} W) was brought into operation by Spinka and Haefner [35-36], which is located in the Czech Republic and which was created by specialists from the Laurence Livermore National Laboratory. The first of the four lines delivered pulses with an energy of 100 mJ and a duration of ~ 20 fs; the repetition rate in the first version was 1 kHz. By 2020, the pulse repetition rate was 10 kHz. At point, the system is being developed that will provide a repetition rate of the order of 100 kHz or higher.

References

[1] Barty A. *et. al*. 2008 *Nat. Photonics* 2, 415-417.

[2] Marchesini S. 2008 *Nat. Photonics*. 2, 560-562.

[3] T. Wang *et. al.* 2012 *Phys. Rev Lett.* 108, 267403.

[4] Ribic P. R., Margaritondo G. 2012 *J. Phys. D: Appl. Phys.* 45, 213001.

[5] Saldin E. L., Schneidmiller E. A., Yurkov M. V. 2010 *Physical Review Special Topics – Accelerators and Beams* 23, 030701.

[6] Chou M.-C, Lin P.-H., Lin C.-A., Lin J.-Y., Wang J., Chen S.-Y. 2007 *Phys. Rev. Let*. 99, 063904.

[7] Lin P.-H., Chou M.-C., Jiang M.-J., Tseng P.-C., Chu H.-H., J.-Y. Lin J.-Y., Wang J., S.-Y. Chen S.-Y. 2009 *Opt. Lett.* 34, 3562-3564.

[8] Chu H.-H., Tsai H.-E., Chou M.-C., Yang L.-S., Lin J.-Y., Lee C.-H., Wang J., S.-Y. Chen S.-Y. 2005 *Phys. Rev. A* 71, 061804.

[9] Chen B.-K. *et al* 2012 *Appl. Phys. B* 106, 817-821.

[10] Ivanova E. P. 2011 *Phys. Rev. A* 84, 043824-1-10.

[11] Ivanova E. P. 2012 *Quantum Electron.* 42, 1100-5.

[12] Mocek T., Sebban S. *et al* 2005 *Phys. Rev. Let.* 95, 173902.

[13] Ivanova E. P., Vinokhodov A. Yu. 2013 *Quantum Electronics* 43 1099-6.

[14] Sebban *et. al.* 2018 *Plasma Phys. Control Fusion* 60, 014030.

[15] Nilsen J. 1997 *J. Opt. Soc. Am. B* 14 1511-1514.

[16] Nilsen J., Dunn J., Osterheld A. L., Li Y. 1999 *Phys. Rev. A* 60, R2677-80.

[17] Fill E. E. 1988 *J. Quant. Spectrosc. Radiat. Transfer* 39, 489-91.

[18] Kuba J., Klisnick A., Ros D., Fourcade Paul, Jamelot G., Miquel J.-L., Blanchot N., Wyart J.-F. 2000 *Phys. Rev A* 62, 043808.

[19] Siegrist M., Jia F., Balmer J. Proceedings of the conference *X-ray lasers 2014*, *Springer Proceedings in Physics*, 169, 89, edited by J. Rocca et al.

[20] Ivanova E. P. 2017 Atoms 5, 25-34.

[21] Ivanova E. P. 2014 *Optics and Spectroscopy* 117, 167-175.

[22] Whitney K. J., Dasgupta A., Pulsifer P. E. 1994 *Phys. Rev. E* 50, 468-71.

[23] Kim C. M., Janowitz A., Kim H. T., and Lee J. *Phys. Rev. A* 2009 80 053811.

[24] Ivanov L. N., Ivanova E. P., Knight L. V. 1993 *Phys. Rev. A* 48 4365-4378.

[25] Ivanov L. N., Ivanova E. P., Knight L. V., Molchanov A. G. 1996 *Physica Scripta* 53 653-667.

[26] Ivanova E. P., Zinoviev N. A. 2001 *J. Phys. IV. France* 11, Pr2-151-4.

[27] McPherson A. *et al* 1994 *Nature (London)* 370, 631-4.

[28] Shao Y. L., Ditmire T., Tisch J. W. G., Springate E., Marangos J. P., and Hutchinson M. H. R. 1996 *Phys. Rev. Lett.* 77, 3343-6.

[29] Ditmire T., Tisch J. W. G., Springate E., Mason M. B., Hay N., Smith R. A., Marangos J., and Hutchinson M. H. R 1997 *Nature (London)* 386, 54-57.

[30] Ditmire T., Smith R. A., Marjoribanks R. S., Kulcsar G., and Hutchinson M. H. R. 1997 *Appl. Phys. Lett.* 71, 166-9.

[31] Hagena O. F. and Obert W. 1972. *J. Chem Phys.* 56, 1793-98.

[32] Chen G., Kim B., Ahn B., and Kim D. E. 2009 *J. Appl. Phys.* 106, 053507.

[33] Springate E., Hay N., Tisch J. W. G., Mason M. B., Ditmire T., Hutchinson M. H. R., Marangos J. P. 2000 *Phys. Rev. A.* 6, 063201.

[34] Ter-Avetisyan S., Vogt U., Stiel H., Schnürer M., Will I., and Nickles P. V. 2003 *J. Appl. Phys.* 94, 5489-95.

[35] Spinka T. M., Haefner C. 2017 *Optics and Photonics* High Repetition Rate *Advanced Petawatt Laser System (HALPS)* p. 28.

[36] Haefner C. L. 2017 High average power, diode pumped petawatt laser systems. A new generation of lasers enabling precision science and commercial applications *Proc. SPIE* 10241 1024102.